

Performance enhancement of dye-sensitized solar cells via co-sensitization of ruthenium (II) based N749 dye and organic sensitizer RK1



M. Younas, K. Harrabi*

Department of Physics, King Fahd University of Petroleum & Minerals (KFUPM), P.O. Box 5047, Dhahran 31261, Saudi Arabia

ARTICLE INFO

Keywords:

Ruthenium (II) based dye (N749)
Organic Sensitizer (RK1)
Co-sensitization
DSSC
Photovoltaic
Efficiency

ABSTRACT

The aim of the reported study is to enhance the photovoltaic performance of a dye-sensitized solar cells (DSSCs) using co-sensitization approach and investigate how the concentration of an organic co-sensitizer influence the overall efficiency of the fabricated DSSCs. The overall efficiency of the fabricated DSSC with co-sensitization approach using a ruthenium (II) based dye, N749, and an organic sensitizer, RK1, is 8.15%. The solar cells were evaluated using UV–Vis spectroscopy, electrochemical impedance spectroscopy (EIS), incident photon to electron conversion efficiency (IPCE), and current-voltage (I-V) characteristics. The concentration of the organic co-sensitizer has a strong effect on the performance of the DSSC. An optimized solar cell fabricated with a dye solution of 0.2 mM RK1 and 0.3 mM N749 yielded a J_{sc} (mA/cm²) = 19.45, V_{oc} (mV) = 688, FF (%) = 61 and power conversion efficiency (PCE) of η (%) = 8.15 under standard (AM1.5 G) 1 sun illumination (100 mW/cm²). The efficiency of co-sensitized DSSCs is far better than the efficiency of fabricated solar cells sensitized with individual dyes [N749 (η = 4.94%) and RK1 (η = 5.76%)]. The efficiency enhancement is due to the lower rate of recombination of electrons and holes, decreased I^-/I_3^- competitive absorption, and lower aggregation of the dyes resulting from the synergistic action in the co-sensitized photovoltaic cells.

1. Introduction

An uninterrupted and reliable energy supply is crucial for the development, modernization through automation, and economic growth of any country. Rising demand for energy and environmental issues have motivated researchers to pursue new eco-friendly and clean energy sources (Younas et al., 2019). Sun's energy is the most easily accessed and most widely available renewable energy source on earth. Accessible estimated annual energy from the sun received by the earth is about 3×10^{24} J, which is about 10^4 times the current energy consumption by all inhabitants of the world (Mehmood et al., 2016b, 2014). Energy from the sun is a leading candidate among the alternative energy sources that can be harnessed to reduce the emission of carbon-based greenhouse gases to the environment due to the use of fossil fuels (Barnham et al., 2006; Canadell et al., 2007; Yang et al., 2014; Younas et al., 2018a). Increase of the CO₂ emissions into the atmosphere is associated with many catastrophic consequences such as global warming, reduction in forest cover, and climate change. Since 1954, various types of solar cells have been developed to harness solar energy. Dye-sensitized solar cells (DSSCs) are novel photovoltaic devices considered to be the third generation of solar cells (Mansha et al., 2019; Yan and Saunders, 2014). Pioneering work of Grätzel and co-

workers in 1991 resulted in the introduction of DSSCs, which have received considerable interest due to their low cost, ease of fabrication, and low toxicity. However, their power conversion efficiency (PCE) is moderate compared to that of the solar cells based on silicon (O'Regan and Grätzel, 1991).

DSSCs consist of three major components: (1) a photoanode, (2) a counter electrode, and (3) an electrolyte. The photoanode is a key component of a DSSC, and it performs the following significant functions; (i) collect electrons released by the dye after photo-excitation and transport them to the current-carrying circuit, and (ii) facilitate the adsorption of the dye by acting as a scaffolding. Typically, anodes have a porous morphology for the adsorption of an adequate quantity of the dye and they are fabricated using materials with a wide band gap, e.g., TiO₂, ZnO, Nb₂O₅ etc. (Yeoh and Chan, 2017). The counter electrode (CE) performs the following key functions: (i) reduce the electrolyte oxidized by the regeneration of the dye, and (ii) attract holes towards the CE. A wide range of materials have been used to fabricate CEs for DSSCs, including carbon nanotubes (CNT), platinum (Pt), and other carbon-based materials etc. (Ahmed et al., 2018; Ehsan et al., 2019; Mehmood et al., 2020, 2019, 2018; Wei et al., 2017). The electrolyte is a crucial component of a DSSC, and it is typically placed between the photoanode and the CE. Regeneration of the photo-excited dye is the

* Corresponding author.

E-mail address: harrabi@kfupm.edu.sa (K. Harrabi).

<https://doi.org/10.1016/j.solener.2020.04.051>

Received 14 February 2020; Received in revised form 5 April 2020; Accepted 18 April 2020

Available online 24 April 2020

0038-092X/ © 2020 International Solar Energy Society. Published by Elsevier Ltd. All rights reserved.

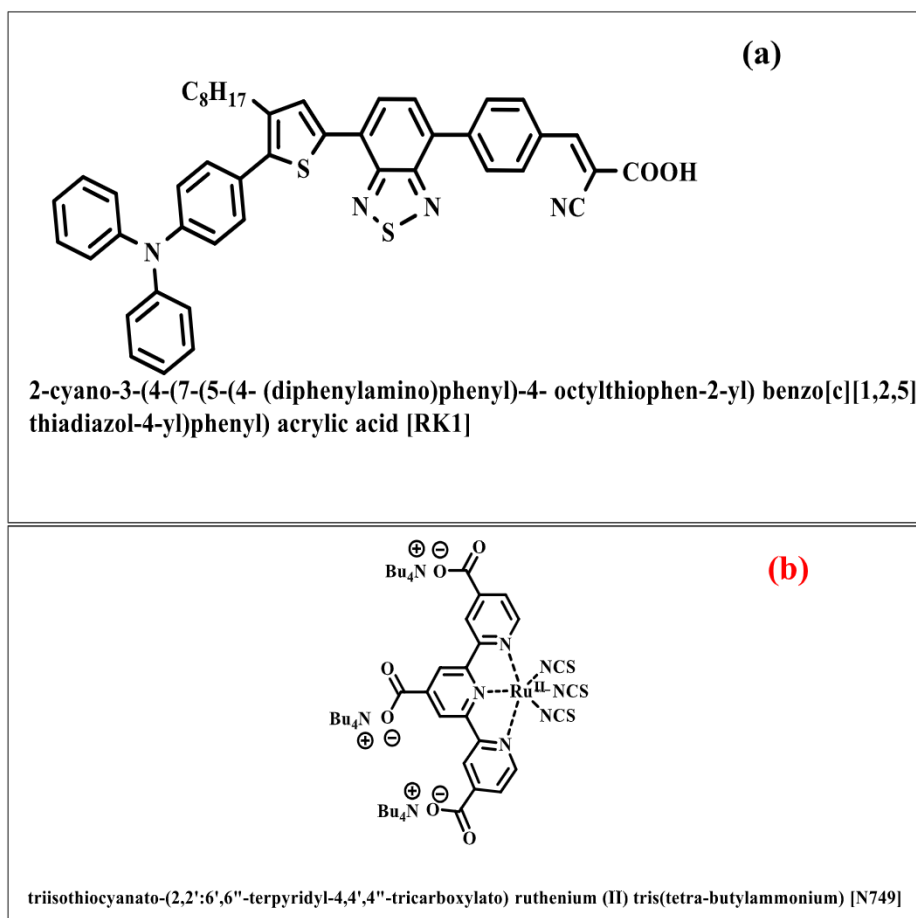


Fig. 1. The structure and chemical name of (a) Organic sensitizer RK1 dye and (b) Ruthenium (II) based N749 dye.

key function of the electrolyte. A wide range of types of electrolytes, e.g., liquids, gel polymers, and other polymers, have been used in DSSCs. The iodide/triiodide (I^-/I_3^-) liquid electrolyte is widely used due to its outstanding characteristics, such as the good solubility, low absorption of light, suitable redox potential, and quick regeneration of the dye. The photosensitizer (dye), which is adsorbed on semiconducting material, such as TiO_2 and ZnO (Younas et al., 2019, 2018a), is the key component of a DSSC. The PCE of a DSSC is governed mainly by the photosensitizer. A dye in a DSSC absorbs photons and produces pairs of electrons and holes that are transferred through the semiconducting material to the external circuit. Many aspects of the DSSC technology have witnessed remarkable progress in the past fifteen years, reaching record efficiencies of over 14% (Kakiage et al., 2015). However, the efficiency of these photovoltaic devices must be further enhanced to promote their large-scale commercial utilization. The narrow absorption range of the photosensitizer (dye) is the main reason for the low PCE of DSSCs (Hagfeldt et al., 2010; Mehmood et al., 2015a). Currently, a single sensitizer that can absorb solar energy in a broad spectrum ranging from 400 to 900 nm is not available (Yum et al., 2007).

Co-sensitization has been shown to enhance the PCE of a DSSC by overcoming the limitation imposed by the narrow spectral range of individual sensitizers (Younas et al., 2018b). Broadened absorption spectral range of a DSSC enhances the efficiency of solar cells (Lan et al., 2012). Researchers have used a wide array of combinations of photosensitizers, such as porphyrin co-sensitized using ruthenium complexes (Wu et al., 2012), an organic dye co-sensitized using ruthenium complexes (Abdellah et al., 2019; Naik et al., 2018), phthalocyanine co-sensitized using an organic sensitizer (Clifford et al., 2011; Jin et al., 2013; Kimura et al., 2012), and an organic sensitizer co-

sensitized using different organic dyes (Chen et al., 2005; Kuang et al., 2007) to enhance the PCE. Kuang et al. obtained a PCE of 6.4% with SQ1 and JK2 organic dyes, and a solvent-less electrolyte (Kuang et al., 2007). Chen et al. employed several dyes for co-sensitization, including a dye based on hemicyanine, a merocyanine dye, and a squarylium cyanine dye and achieved 6.5% PCE (Chen et al., 2005). Wu et al. synthesized and used two organic dyes based on indolium in a 1:3 ratio and obtained a 3.0% PCE for standard 1 sun AM 1.5G illumination (Wu et al., 2009). Lee et al. employed the co-sensitization technique with DSSCs fabricated with plastic and achieved 5.1% PCE. They co-sensitized N719 and N749 ruthenium complexes with thienylfluorene segment containing organic dye known as FL (Lee et al., 2011). Lan et al. used an organic sensitizer (CD5) to co-sensitize a zinc porphyrin dye (LD12) in a stepwise manner reaching a 9% PCE (Lan et al., 2012). Wei et al. co-sensitized three organic dyes (DM, DE, and DP) with a ruthenium dye (N719) and achieved a 7% PCE (Wei et al., 2013). It is pertinent to mention here, for pure RK1 dye the efficiency obtained by D. Joly et al. is different from our achieved efficiency using same dye RK1, due to huge difference in fabrication process and conditions. The difference includes twice $TiCl_4$ treatment, scattering layer, shedding mask, different heat treatment, different CE fabrication process and most importantly less active area (i.e. 0.16 cm^2) (Joly et al., 2015).

In this study, co-sensitization is used to boost the efficiency of DSSCs. The semiconductor anode is sensitized using solutions with different concentrations of the organic RK1 dye and ruthenium (II) based dye N749. The performance of DSSCs based on a single dye (N749 or RK1) is compared with that of co-sensitized DSSCs based on N749 and RK1 dyes using the identical conditions. The performance of the co-sensitized solar cells functioning at an optimum level is significantly better than that of the photovoltaic cells based on a single

dye, yielding a much superior PCE.

2. Fabrication and characterization

2.1. Materials

Dyes (21822; Ruthenizer 620-1H3TBA, and 22751; Sensitizer RK1), electrolyte (35112; Iodolyte Z-50), anatase TiO₂ paste (14412; T/SP), platinum paste (Plastisol T) and fluorine-doped tin oxide (SnO₂:F) FTO conductive glass substrate, were obtained from Solaronix (Switzerland).

2.2. Preparation of the dye solutions

Two solutions of the individual dyes and five solutions of the mixtures of the dyes in ethanol were prepared at the following concentrations: (i) 0.5 mM N749, (ii) 0.4 mM N749 and 0.1 mM RK1, (iii) 0.3 mM N749 and 0.2 mM RK1, (iv) 0.25 mM N749 and 0.25 mM RK1, (v) 0.2 mM N749 and 0.3 mM RK1, (vi) 0.1 mM N749 and 0.4 mM RK1, and (vii) 0.5 mM RK1. The chemical name and the structure of the dyes are shown in Fig. 1.

2.3. Fabrication of the DSSCs

A schematic representation of a DSSC and its energy band diagram are depicted in Fig. 2a and b, respectively. Tape casting was used to apply TiO₂ paste on the FTO conductive glass substrates and it was annealed at 200 °C for the first 10 min and 450 °C for the next 20 min to fabricate the mesoporous scaffolding layer for photoanodes. SEM cross-sectional images shown in Fig. 3 were used to determine the thickness of the deposited TiO₂ films on each substrate. The TiO₂ films of the photoanodes have an average thickness of 5.6 μm. The photoanodes were prepared by soaking the FTO conductive substrates deposited with

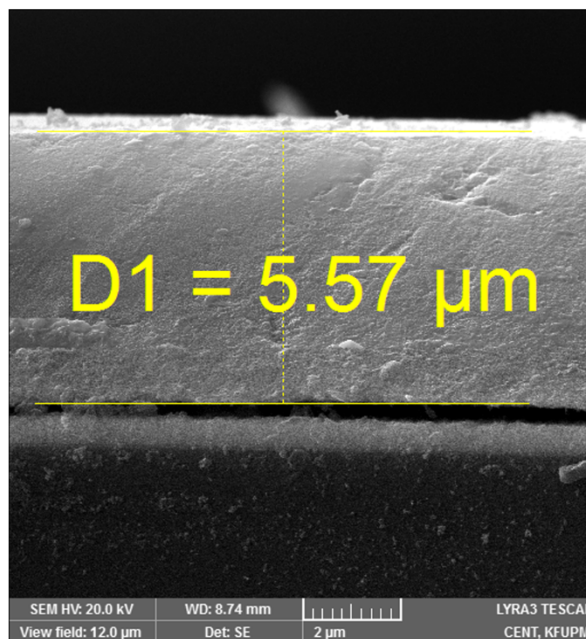


Fig. 3. A cross-sectional image of the TiO₂ film deposited on an FTO glass substrate.

TiO₂ layer for 24 h into dye solutions. The unadsorbed dye was removed by rinsing the photoanodes with ethanol after soaking. The platinum counter electrodes were also fabricated using platinum paste with similar tape casted on to the FTO glass substrates and annealing at 450 °C for 30 min. The two electrodes were attached to each other using super glue gel (from the super glue corporation). Subsequently, the space between the two electrodes was filled with the electrolyte to fabricate the DSSCs. The DSSCs used in this study have an active area of 0.2 cm².

2.4. Characterization of the anodes and DSSCs

A model UV/Vis JASCO-670 spectrophotometer was used to characterize the solutions containing the dyes as well as the dyes anchored to TiO₂ films. Cross-sectional images of the anodes captured using a field emission scanning electron microscope (FE-SEM, TESCON Lyra-3), were used to determine the thickness of the prepared TiO₂ thin films. The IV characteristics of the fabricated DSSCs were evaluated using a solar simulator (IV-5, PV Measurements) at an Air Mass (AM) of 1.5 G (1000 Wm⁻²) with a Source Meter (Keithley 2400). Electrochemical impedance spectroscopic (EIS) analysis of the DSSCs was performed using a BioLogic Sciences Instruments potentiostat (VMP3) under dark conditions of illumination and an AC signal with a frequency between 10 Hz and 800 KHz and an amplitude of 10 mV. A bias between 0 and 750 mV, which is larger than the V_{oc} of the DSSC, was applied in the EIS analysis.

3. Results and discussion

3.1. Ultraviolet and visible spectroscopic analysis of the fabricated DSSCs

The ultraviolet–visible (UV–Vis) absorption spectra of the individual dyes N749 and RK1 as well as their mixtures in both ethanol and adsorbed on the TiO₂ films on the FTO substrate are shown in Fig. 4. The UV–Vis spectra of N749 shown in Fig. 4b have three broad and intense peaks at 610, attributed to metal-to-ligand charge transfer (MLCT) and at 410, and 340 nm attributed to the intraligand (π–π*) charge-transfer transitions. As also shown in Fig. 4b, the UV–Vis spectrum of RK1 has absorption peaks at wavelengths ranging from 398 to 536 nm and

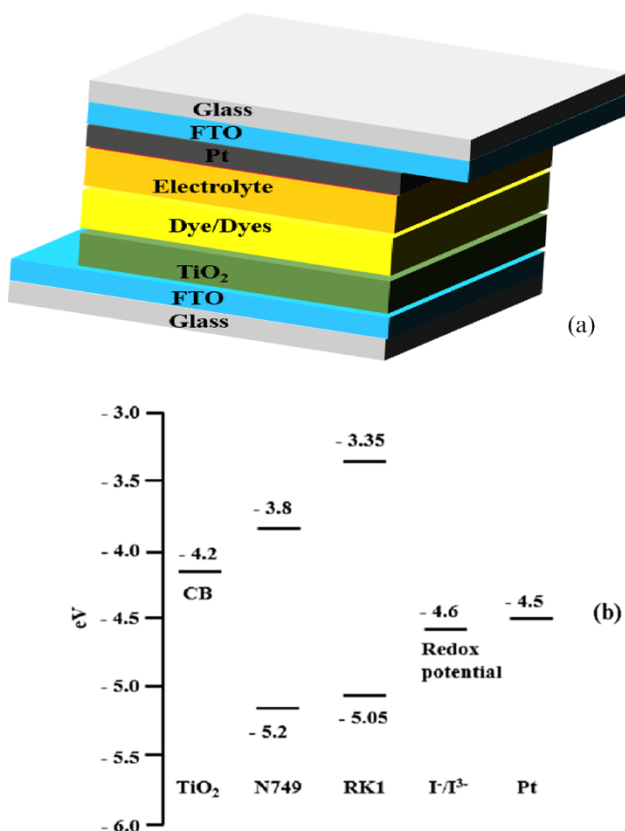


Fig. 2. (a) Schematic representation of the components of a DSSC and (b) Energy band diagram of a DSSC.

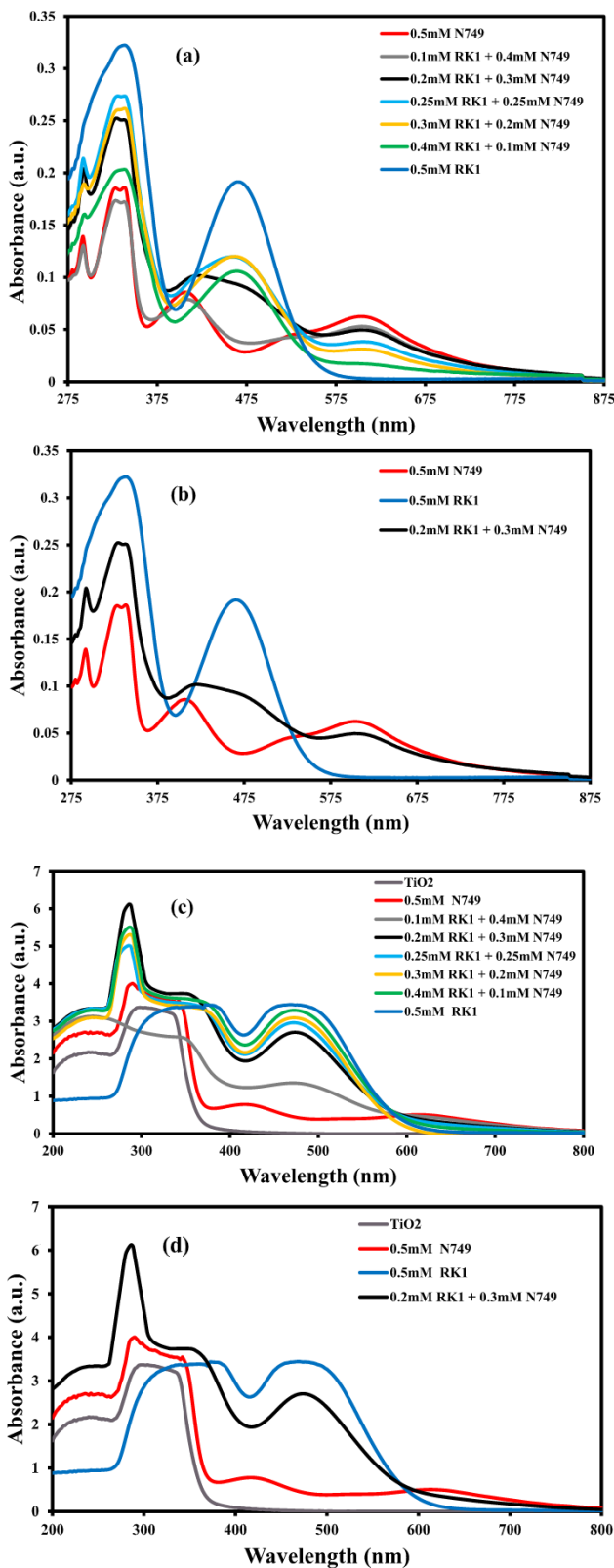


Fig. 4. UV-Vis spectra of (a) Pure N749, pure RK1, and mixtures of RK1 and N749 in EtOH; (b) Pure N749, pure RK1, and the best performing mixture of 0.2 M RK1 and 0.3 M N749 in EtOH; (c) Pure N749, pure RK1, and mixtures of RK1 and N749 adsorbed on TiO₂ thin films; and (d) Pure N749, pure RK1, and the best performing mixture of 0.2 M RK1 and 0.3 M N749 adsorbed on a TiO₂ thin film.

286–372 nm. The peak in the 286–372 nm region is attributed to the π - π^* transition of the conjugated bonds, while the other peak is due to the intermolecular charge transfer (ICT) from the anchoring group acting as the donor to the anchoring group acting as the acceptor. The peaks in the absorption spectra of the mixed dyes in ethanol shown in Fig. 4a are broader and more intense than that of N749 alone. The spectra show that the concentration of RK1 has a significant effect on the absorption of light by N749. Absorption of light by N749 is considerably boosted with the concentration increase of the RK1 sensitizer owing to the synergistic effect of the two dyes. However, the π^* orbital delocalization when the surface Ti⁴⁺ ions interact with the carboxylate groups (Mehmood et al., 2015c), shifts the absorption of the mixtures of N749 and RK1 towards longer wavelengths when anchored on TiO₂, as shown in Fig. 4d. Specifically the peaks are red shifted from 610 nm to 628 nm as indicated in Fig. 4c and d. Furthermore, the peaks at 284 nm and 478 nm in the UV-Vis spectrum of the mixture of N749 and RK1 dyes adsorbed on TiO₂ is sharper and more intense compared to the same peak of N749 anchored on TiO₂ under the same conditions. The results clearly demonstrate that the TiO₂/(N749 + RK1) thin films absorb more energy from light they receive compared to that of TiO₂/N749 or TiO₂/RK1 films due to co-sensitization. The increased absorption of photons increases the available conduction electrons, leading to a higher current density and a better efficiency.

To estimate the dyes loading on the photoanode of TiO₂, samples TiO₂/N749, TiO₂/RK1, and TiO₂/0.2 mM RK1 + 0.3 mM N749 sensitized with N749, RK1 and 0.2 mM RK1 + 0.3 mM N749 respectively were placed into a 20 mM KOH solution and stirred at room temperature for 24 h to desorb the dyes. The concentrations of the desorbed dyes were determined by using UV-vis spectroscopy (Han et al., 2010). For this purpose, calibration curves were plotted for N749 (0.5 mM), RK1 (0.5 mM) and 0.2 mM RK1 + 0.3 mM N749 solutions by making series dilutions ranging from 0.5 mM to 0.0078 mM. In each calibration curve the value of coefficient of determination (R^2) was maintained > 0.999. The total amount of N749 obtained after desorption of TiO₂/N749 solar cell was found 0.093 mM per 0.20 cm² area. Similarly, from the desorption of TiO₂/RK1, and TiO₂/0.2 mM RK1 + 0.3 mM N749 the total calculated amounts of RK1 and 0.2 mM RK1 + 0.3 mM N749 were found 0.139 mM and 0.184 mM respectively.

3.2. Determination of the I-V characteristics of the fabricated DSSCs

Fig. 5 depicts the I-V plots of the fabricated co-sensitized solar cells and Table 1 provides their photovoltaic parameters. Values of the open circuit voltage (V_{oc}), current density (J_{sc}), and efficiency (η), and the fill factor (FF) of the fabricated DSSCs are provided in Table 1. The results in Table 1 clearly indicate that the current density of the

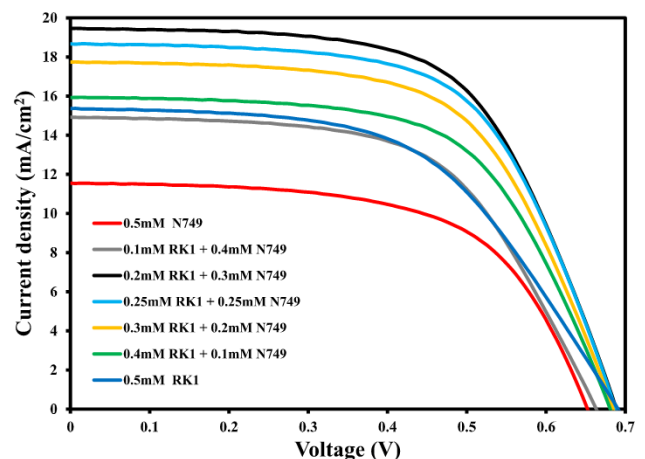


Fig. 5. Current-voltage characteristics of DSSCs.

Table 1
Current-voltage characteristics of the fabricated solar cells.

| Cell structure | J_{sc} (mA/cm ²) | V_{oc} (mV) | FF (%) | η (%) | R_1 (Ohm) |
|----------------------------|--------------------------------|---------------|--------|------------|-------------|
| 0.5 mM N749 | 11.55 | 652 | 60 | 4.54 | 28 |
| 0.1 mM RK1 + 0.4 mM N749 | 14.92 | 663 | 60 | 5.94 | 25 |
| 0.2 mM RK1 + 0.3 mM N749 | 19.45 | 688 | 61 | 8.15 | 9 |
| 0.25 mM RK1 + 0.25 mM N749 | 18.66 | 687 | 61 | 7.88 | 14 |
| 0.3 mM RK1 + 0.2 mM N749 | 17.73 | 685 | 61 | 7.37 | 15 |
| 0.4 mM RK1 + 0.1 mM N749 | 15.93 | 681 | 61 | 6.16 | 16 |
| 0.5 mM RK1 | 15.36 | 691 | 54 | 5.76 | 27 |

photovoltaic cells increases up to the optimized concentration. Above the optimized concentration of RK1 the current density decreases as the number of available electrons at higher concentrations of RK1 decreases due to the elevated bandgap of the organic dye (Fig. 2b). The fill factor and the open circuit voltage also increase up to the optimized concentrations of the dyes and then decrease. The performance of the DSSCs is enhanced by co-sensitization both by achieving the highest absorption owing to the larger absorption coefficient of the organic dye and higher current due to the smaller band gap of the ruthenium-based dye. As indicated by the data obtained, the performance of the co-sensitized DSSCs depends strongly on the concentration of the co-sensitizer. A solar cell sensitized with 0.2 mM RK1 and 0.3 mM N749 has a J_{sc} of 19.45 mA/cm², V_{oc} of 688 mV, FF of 61%, and η of 8.15% under optimized conditions. The value of PCE of the co-sensitized DSSC is significantly higher compared to the devices sensitized by individual dyes (TiO₂/N749 or TiO₂/RK1). The PCE of the co-sensitized solar cells are enhanced mainly due to the increase in J_{sc} (19.45 mA cm⁻²), fill factor (61%), and V_{oc} (688 mV). J_{sc} is increased primarily due to the significantly high absorption of light, and the major cause of the increase of V_{oc} is due to the suppression of charge recombination by co-sensitization.

3.3. IPCE analysis of the fabricated DSSCs

The incident photon to electron conversion efficiency (IPCE) is basically the measurement of external quantum efficiency (EQE) of the fabricated solar cell devices over a specific wavelength range. In other words this explains the efficient workability of the fabricated solar cells devices in that particular wavelength region. Basically IPCE or EQE is the ratio between total numbers of electrons generated in response to the total number of photon falling on the active area of the fabricated solar cell device. The IPCE is a strong function of wavelength due to various wavelength dependent factors as provide in the Eq. (1) below.

$$IPCE(\lambda) = LHE(\lambda) * \varphi_{inj} * \eta_{cc} \quad (1)$$

Eq. (1) shows the IPCE (λ) depends on the light harvesting efficiency (LHE) which is highly depended on wavelength. Secondly, the IPCE depends on φ_{inj} , which represent the amount of injection of photo-generated electrons from excited dye to the conduction band of the semiconductor. Finally the third factor is called collection efficiency of the photo-generated electrons and it is represented as η_{cc} in the Eq. (1) (Grätzel, 2005).

Fig. 6 shows IPCE spectra of all the seven DSSC devices fabricated in this work. The IPCE (EQE) spectral response for pure N749 and RK1 are clearly different with the highest peaks showing at different wavelengths. However, from all other co-sensitized IPCE spectral curves the curves showing feathers from both dyes which experimentally proving its co-sensitization and grabbing various wavelength for co-sensitized IPCE peaks.

Furthermore, LHE (λ) depends on three factors (1) the light scattering at the photo-anode, (2) the dye adsorption on the surface of the

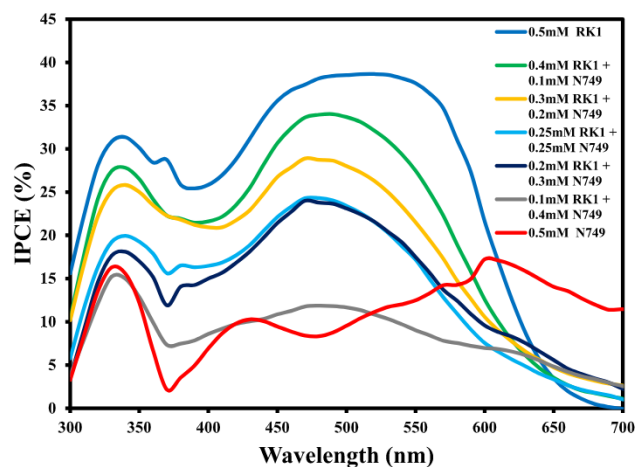


Fig. 6. Incident photo to electron conversion efficiency (IPCE) of fabricated DSSCs.

semiconductor, and (3) the light absorbance characteristics of the dye. The resemblance of IPCE spectrum in Fig. 6 to the absorbance spectrum in Fig. 4c and the observation of an optimum co-sensitization contents of the dyes (N749 and RK1) in Figs. 4, 5, and 6 indicate these dependences of LHE (λ). Also, the co-sensitization promotes the injection of photo-excited electron in the co-sensitized dyes to the conduction band of semiconductor i.e. TiO₂, resulting in the increase of φ_{inj} and contributing positively to IPCE (λ) (Yang et al., 2016). The third parameter in the Eq. (1) i.e. electron collection efficiency (η_{coll}) is linked with the charge recombination and charge transport properties of the semiconducting anode, which can be explained by electrochemical analysis. In our case the electrochemical analysis shows that the co-sensitized DSSCs are better than pure dyes DSSCs and the charge transfer resistance (R_1) at counter electrode/electrolyte is much less than the pure dyes devices, which clearly proving the less charge recombination at photoanode/electrolyte interface is in good agreement with IPCE spectra.

3.4. Electrochemical impedance spectroscopic analysis of the fabricated DSSCs

Charge recombination in DSSCs is a major shortcoming which affects their performance. Charge recombination occurs when the electrons generated by the incident photons recombine with the holes in the excited dye molecules, rather than moving to the conduction band (CB) of the porous semiconductor to be harvested by the external circuit. The electrons can also recombine with the holes generated in the excited dye molecules when in the semiconductor or with the ionized electrolyte atoms (Ondersma and Hamann, 2013). In this study, the resistance to charge recombination in the DSSCs was evaluated using EIS analysis. Fig. 7 shows the EIS spectra (Nyquist plots) of the solar cells and their equivalent circuit (inset Fig. 7). In an EIS spectrum the first of the three semicircles at higher frequencies is results from the charge transfer resistance, i.e., the interfacial resistance at the counter electrode and the electrolyte interface (R_1). The second arc at intermediate frequency represents the interfacial resistance between the photoanode and the electrolyte (R_2), and the third arc at low frequency represents the resistance to carrier transport, i.e., the redox couple diffusion, in the electrolyte (Z_w) (Mehmood et al., 2016a). In the equivalent circuit of the DSSC depicted in Fig. 7 (inset), R_s is the value of the resistance at the beginning of the first arc at higher frequencies in the EIS plot, i.e., the series resistance. The resistance R_1 represents the interfacial resistance at back electrode/electrolyte interface and the resistance R_2 represents the recombination rate at the anode/electrolyte interface. C_1 and C_2 are the capacitances (constant phase elements) at the counter

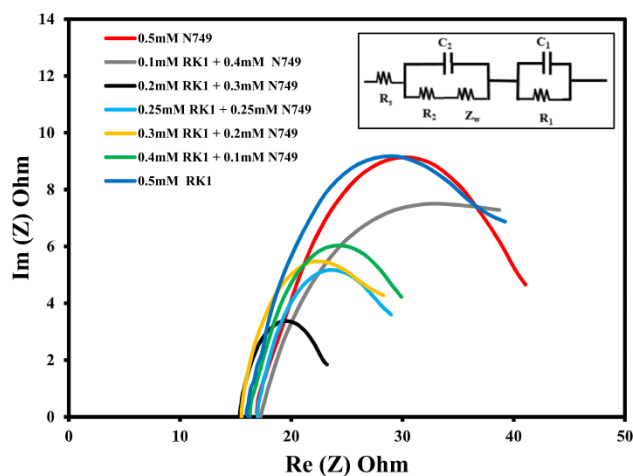


Fig. 7. Electrochemical impedance spectroscopic analysis of fabricated DSSCs and the equivalent circuit of a DSSC (inset).

electrode/electrolyte interface and the anode/electrolyte interface, respectively. Warburg diffusion impedance is represented by Z_w . In the Nyquist plots of the DSSCs depicted in Fig. 7, only the first arc due to the electrolyte/counter electrode interfacial resistance (R_1) is visible. The two remaining smaller arcs may be hidden by the first arc (Li et al., 2010; Nair et al., 2011). Moreover, the resistance to free-carrier recombination at the interface of the anode and the electrolyte (R_2) represents one of the smaller arcs (Mehmood et al., 2016a, 2015a). The electron lifetime is higher when the recombination resistance of free carriers is larger, and vice versa (Mehmood et al., 2015b). The values of the charge transfer resistance of the fabricated DSSCs are listed in Table 1. The results depicted in Fig. 7 and listed in Table 1 indicate that R_1 of the sensitized DSSC with the composition 0.2 mM RK1 and 0.3 mM N749 has the lowest resistance to the flow of free charges originating in the outer circuit, which take part in the reduction of the oxidized electrolyte. Thus, the efficiency of the co-sensitized DSSCs is increased due to the longer electron transport lifetime resulting from the synergetic effect of co-sensitization by N749 and RK1. The effectiveness of co-sensitization is confirmed by the results in Table 1, which indicate that the individual dyes have a higher charge transfer resistance compared to that of the DSSCs based on the co-sensitized configuration. Enhancement of the coverage of the surface of TiO_2 by the dyes due to co-sensitization increases the electron lifetime. When the surface coverage by the dyes is high, the chances of the electrons interacting with TiO_2 are lowered, thereby reducing the recombination process. Also, the higher coverage of the TiO_2 surface by the dyes will generate more electrons and reduce charge recombination due to the direct exposure of the TiO_2 surface to the electrolyte, thereby improving the PCE of the photovoltaic cells based on the co-sensitized configuration.

4. Conclusion

In this study, the performance of a DSSC was improved using co-sensitization. Organic sensitizer RK1 was used as the co-sensitizer with N749, a dye based on ruthenium (II). Mixed dye solutions at five different concentrations of the two dyes as well as solutions of the individual dyes were used to fabricate the DSSCs. The fabricated DSSCs were characterized using the following techniques; (i) UV–Vis spectroscopy, (ii) I–V characteristics determination, incident photon to electron conversion efficiency (IPCE), and (iii) EIS analysis. Main findings of the study are as follows:

- The results of the study demonstrate that co-sensitization is highly effective in boosting the overall PCE of a DSSC.

- The spectra indicate that absorption by the dye solutions in the UV–Vis region becomes higher with increasing RK1 content. However, the peaks in the UV–Vis spectra also become more intense and broader when the dyes are anchored to the FTO surface coated with a TiO_2 film.
- The PCE, V_{oc} , J_{sc} , FF, and the charge transfer resistance of the photovoltaic cells display a very high dependence on the concentration of the RK1 dye. A solar cell fabricated with 0.2 mM RK1 and 0.3 mM N749 has a PCE of 8.15% when tested using optimized conditions. This is significantly higher than a solar cell sensitized using individual dyes (N749 = 4.54% and RK1 = 5.76%).
- The results also confirm that the resistance to charge transfer across the interface of the electrolyte/counter electrode decreases with co-sensitization, which reduces the dark current and increases the current density enhancing the overall efficiency of the photovoltaic cell.

Declaration of Competing Interest

None.

Acknowledgement

M.Y and K.H would like to thank the National Science, Technology and Innovation Program of KACST for funding this research under Project No. 12-ENE2379-04. They also acknowledge support from KFUPM and Research Institute.

References

- Abdellah, I.M., Koraiem, A.I., El-Shafei, A., 2019. Molecular engineering and investigation of new efficient photosensitizers/co-sensitizers based on bulky donor enriched with EDOT for DSSCs. Dye. Pigment. 164, 244–256. <https://doi.org/10.1016/j.dyepig.2019.01.035>.
- Ahmed, U., Alizadeh, M., Rahim, N.A., Shahabuddin, S., Ahmed, M.S., Pandey, A.K., 2018. A comprehensive review on counter electrodes for dye sensitized solar cells: a special focus on Pt-TCO free counter electrodes. Sol. Energy 174, 1097–1125. <https://doi.org/10.1016/j.solener.2018.10.010>.
- Barnham, K.W.J., Mazzer, M., Clive, B., 2006. Resolving the energy crisis: nuclear or photovoltaics? Nat. Mater. 5, 161–164. <https://doi.org/10.1038/nmat1604>.
- Canadell, J.G., Le Quere, C., Raupach, M.R., Field, C.B., Buitenhuis, E.T., Ciais, P., Conway, T.J., Gillett, N.P., Houghton, R.A., Marland, G., 2007. Contributions to accelerating atmospheric CO₂ growth from economic activity, carbon intensity, and efficiency of natural sinks. Proc. Natl. Acad. Sci. 104, 18866–18870. <https://doi.org/10.1073/pnas.0702737104>.
- Chen, Y., Zeng, Z., Li, C., Wang, W., Wang, X., Zhang, B., 2005. Highly efficient co-sensitization of nanocrystalline TiO_2 electrodes with plural organic dyes. New J. Chem. 29, 773. <https://doi.org/10.1039/c0jm03661g>.
- Clifford, J.N., Forneli, A., Chen, H., Torres, T., Tan, S., Palomares, E., 2011. Co-sensitized DSSCs: dye selection criteria for optimized device Voc and efficiency. J. Mater. Chem. 21, 1693. <https://doi.org/10.1039/c0jm03661g>.
- Ehsan, M.A., Younas, M., Rehman, A., Altaf, M., Khan, M.Y., Al-Ahmed, A., Ahmad, S., Isab, A.A., 2019. Synthesis and utilization of platinum(II) dialkylthiocarbamate precursors in aerosol assisted chemical vapor deposition of platinum thin films as counter electrodes for dye-sensitized solar cells. Polyhedron 166. <https://doi.org/10.1016/j.poly.2019.03.058>.
- Grätzel, M., 2005. Solar energy conversion by dye-sensitized photovoltaic cells. Inorg. Chem. 44, 6841–6851. <https://doi.org/10.1021/ic0508371>.
- Hagfeldt, A., Boschloo, G., Sun, L., Kloo, L., Pettersson, H., 2010. Dye-sensitized solar cells. Chem. Rev. 110, 6595–6663. <https://doi.org/10.1021/cr900356p>.
- Han, J., Fan, F., Xu, C., Lin, S., Wei, M., Duan, X., Wang, Z.L., 2010. ZnO nanotube-based dye-sensitized solar cell and its application in self-powered devices. Nanotechnology 21, 405203. <https://doi.org/10.1088/0957-4484/21/40/405203>.
- Jin, L., Ding, Z.L., Chen, D.J., 2013. Zinc octacarboxylic phthalocyanine/lutein dyads co-adsorbed nanocrystalline TiO_2 electrode: enhancement in photovoltaic performance of dye-sensitized solar cells. J. Mater. Sci. 48, 4883–4891. <https://doi.org/10.1007/s10853-013-7268-y>.
- Joly, D., Pellejà, L., Narbey, S., Oswald, F., Chiron, J., Clifford, J.N., Palomares, E., Demadrille, R., 2015. A robust organic dye for dye sensitized solar cells based on iodine/iodide electrolytes combining high efficiency and outstanding stability. Sci. Rep. 4, 4033. <https://doi.org/10.1038/srep04033>.
- Kakiage, K., Aoyama, Y., Yano, T., Oya, K., Fujisawa, J., Hanaya, M., 2015. Highly-efficient dye-sensitized solar cells with collaborative sensitization by silyl-anchor and carboxy-anchor dyes. Chem. Commun. 51, 15894–15897. <https://doi.org/10.1039/C5CC06759F>.
- Kimura, M., Nomoto, H., Masaki, N., Mori, S., 2012. Dye molecules for simple co-

- sensitization process: fabrication of mixed-dye-sensitized solar cells. *Angew. Chem. Int. Ed. Engl.* 51, 4371–4374. <https://doi.org/10.1002/anie.201108610>.
- Kuang, D., Walter, P., Nüesch, F., Kim, S., Ko, J., Comte, P., Zakeeruddin, S.M., Nazeeruddin, M.K., Grätzel, M., 2007. Co-sensitization of organic dyes for efficient ionic liquid electrolyte-based dye-sensitized solar cells. *Langmuir* 23, 10906–10909. <https://doi.org/10.1021/la702411n>.
- Lan, C.-M., Wu, H.-P., Pan, T.-Y., Chang, C.-W., Chao, W.-S., Chen, C.-T., Wang, C.-L., Lin, C.-Y., Diao, E.W.-G., 2012. Enhanced photovoltaic performance with co-sensitization of porphyrin and an organic dye in dye-sensitized solar cells. *Energy Environ. Sci.* 5, 6460. <https://doi.org/10.1039/c2ee21104a>.
- Lee, K.-M., Hsu, Y.-C., Ikegami, M., Miyasaka, T., Justin Thomas, K.R., Lin, J.T., Ho, K.-C., 2011. Co-sensitization promoted light harvesting for plastic dye-sensitized solar cells. *J. Power Sources* 196, 2416–2421. <https://doi.org/10.1016/j.jpowsour.2010.10.041>.
- Li, S., Lin, Y., Tan, W., Zhang, J., Zhou, X., Chen, J., Chen, Z., 2010. Preparation and performance of dye-sensitized solar cells based on ZnO-modified TiO₂ electrodes. *Int. J. Miner. Metall. Mater.* 17, 92–97. <https://doi.org/10.1007/s12613-010-0116-z>.
- Mansha, M., Younas, M., Gondal, M.A., Ullah, N., 2019. 1,5-Naphthyridine-based conjugated polymers as co-sensitizers for dye-sensitized solar cells. *Sol. Energy* 194. <https://doi.org/10.1016/j.solener.2019.11.022>.
- Mehmood, U., Ahmed, S., Hussein, I.A., Harrabi, K., 2015a. Co-sensitization of TiO₂-MWCNTs hybrid anode for efficient dye-sensitized solar cells. *Electrochim. Acta* 173, 607–612. <https://doi.org/10.1016/j.electacta.2015.05.132>.
- Mehmood, U., Ahmed, S., Hussein, I.A., Harrabi, K., 2015b. Improving the efficiency of Dye sensitized solar cells by TiO₂-graphene nanocomposite photoanode. *Photon. Nanostruct. - Fundam. Appl.* <https://doi.org/10.1016/j.photonics.2015.08.003>.
- Mehmood, U., Asghar, H., Babar, F., Younas, M., 2020. Effect of graphene contents in polyaniline/graphene composites counter electrode material on the photovoltaic performance of dye-sensitized solar cells (DSSCs). *Sol. Energy* 196, 132–136. <https://doi.org/10.1016/j.solener.2019.12.024>.
- Mehmood, U., Hussein, I.A., Harrabi, K., Mekki, M.B., Ahmed, S., Tabet, N., 2015c. Hybrid TiO₂-multiwall carbon nanotube (MWCNTs) photoanodes for efficient dye sensitized solar cells (DSSCs). *Sol. Energy Mater. Sol. Cells* 140, 174–179. <https://doi.org/10.1016/j.solmat.2015.04.004>.
- Mehmood, U., Hussein, I.A., Harrabi, K., Tabet, N., Berdiyrov, G.R., 2016a. Enhanced photovoltaic performance with co-sensitization of a ruthenium(II) sensitizer and an organic dye in dye-sensitized solar cells. *RSC Adv.* 6, 7897–7901. <https://doi.org/10.1039/C5RA26577K>.
- Mehmood, U., Karim, N.A.N.A., Zahid, H.F., Asif, T., Younas, M., 2019. Polyaniline/graphene nanocomposites as counter electrode materials for platinum free dye-sensitized solar cells (DSSCs). *Mater. Lett.* 256, 126651.
- Mehmood, U., Rahman, S., Harrabi, K., Hussein, I.A., Reddy, B.V.S., 2014. Recent Advances in Dye Sensitized Solar Cells Cells 0–13. <https://doi.org/10.1155/2014/974782>.
- Mehmood, U., Ul Haq Khan, A., Ali Qaiser, A., Bashir, S., Younas, M., 2018. Nanocomposites of carbon allotropes with TiO₂ as effective photoanodes for efficient dye-sensitized solar cells. *Mater. Lett.* 228, 125–128. <https://doi.org/10.1016/j.matlet.2018.05.127>.
- Mehmood, U., Zaheer Aslam, H., Al-Sulaiman, F.A.F.A., Al-Ahmed, A., Ahmed, S., Irfan Malik, M., Younas, M., Aslam, H.Z., Al-Sulaiman, F.A.F.A., Al-Ahmed, A., Ahmed, S., Malik, M.I., Younas, M., 2016b. Electrochemical impedance spectroscopy and photovoltaic analyses of dye-sensitized solar cells based on carbon/TiO₂ composite counter electrode. *J. Electrochem. Soc.* 163, H339–H342. <https://doi.org/10.1149/2.011160jes>.
- Naik, P., Abdellah, I.M., Abdel-Shakour, M., Su, R., Keremane, K.S., El-Shafei, A., Vasudeva Adhikari, A., 2018. Improvement in performance of N3 sensitized DSSCs with structurally simple aniline based organic co-sensitizers. *Sol. Energy* 174, 999–1007. <https://doi.org/10.1016/j.solener.2018.09.071>.
- Nair, A.S., Jose, R., Shengyuan, Y., Ramakrishna, S., 2011. A simple recipe for an efficient TiO₂ nanofiber-based dye-sensitized solar cell. *J. Colloid Interface Sci.* 353, 39–45. <https://doi.org/10.1016/j.jcis.2010.09.042>.
- O'Regan, B., Grätzel, M., 1991. A low-cost, high-efficiency solar cell based on dye-sensitized colloidal TiO₂ films. *Nature* 353, 737–740. <https://doi.org/10.1038/353737a0>.
- Ondersma, J.W., Hamann, T.W., 2013. Recombination and redox couples in dye-sensitized solar cells. *Coord. Chem. Rev.* 257, 1533–1543. <https://doi.org/10.1016/j.ccr.2012.09.010>.
- Wei, L., Yang, Y., Fan, R., Wang, P., Li, L., Yu, J., Yang, B., Cao, W., 2013. Enhance the performance of dye-sensitized solar cells by co-sensitization of 2,6-bis(iminoalkyl)pyridine and N719. *RSC Adv.* 3, 25908. <https://doi.org/10.1039/c3ra44194f>.
- Wei, W., Stacchiola, D.J., Hu, Y.H., 2017. 3D graphene from CO₂ and K as an excellent counter electrode for dye-sensitized solar cells. *Int. J. Energy Res.* 41, 2502–2508. <https://doi.org/10.1002/er.3815>.
- Wu, H.-P., Ou, Z.-W., Pan, T.-Y., Lan, C.-M., Huang, W.-K., Lee, H.-W., Reddy, N.M., Chen, C.-T., Chao, W.-S., Yeh, C.-Y., Diao, E.W.-G., 2012. Molecular engineering of cocktail co-sensitization for efficient panchromatic porphyrin-sensitized solar cells. *Energy Environ. Sci.* 5, 9843. <https://doi.org/10.1039/c2ee22870j>.
- Wu, W., Meng, F., Li, J., Teng, X., Hua, J., 2009. Co-sensitization with near-IR absorbing cyanine dye to improve photoelectric conversion of dye-sensitized solar cells. *Synth. Met.* 159, 1028–1033. <https://doi.org/10.1016/j.synthmet.2009.01.023>.
- Yan, J., Saunders, B.R., 2014. Third-generation solar cells: a review and comparison of polymer/fullerene, hybrid polymer and perovskite solar cells. *RSC Adv.* 4, 43286–43314. <https://doi.org/10.1039/C4RA07064J>.
- Yang, M.-Q., Zhang, N., Pagliaro, M., Xu, Y.-J., 2014. Artificial photosynthesis over graphene-semiconductor composites. Are we getting better? *Chem. Soc. Rev.* 43, 8240–8254. <https://doi.org/10.1039/C4CS00213J>.
- Yang, Y., Zhao, J., Cui, C., Zhang, Y., Hu, H., Xu, L., Pan, J., Li, C., Tang, W., 2016. Hydrothermal growth of ZnO nanowires scaffolds within mesoporous TiO₂ photoanodes for dye-sensitized solar cells with enhanced efficiency. *Electrochim. Acta* 196, 348–356. <https://doi.org/10.1016/j.electacta.2016.03.022>.
- Yeoh, M.-E., Chan, K.-Y., 2017. Recent advances in photo-anode for dye-sensitized solar cells: a review. *Int. J. Energy Res.* 41, 2446–2467. <https://doi.org/10.1002/er.3764>.
- Younas, M., Gondal, M.A., Dastageer, M.A., Baig, U., 2018a. Fabrication of cost effective and efficient dye sensitized solar cells with WO₃-TiO₂ nanocomposites as photoanode and MWCNT as Pt-free counter electrode. *Ceram. Int.* 45. <https://doi.org/10.1016/j.ceramint.2018.09.269>.
- Younas, M., Gondal, M.A., Dastageer, M.A., Harrabi, K., 2019. Efficient and cost-effective dye-sensitized solar cells using MWCNT-TiO₂ nanocomposite as photoanode and MWCNT as Pt-free counter electrode. *Sol. Energy* 188, 1178–1188. <https://doi.org/10.1016/j.solener.2019.07.009>.
- Younas, M., Gondal, M.A., Mehmood, U., Harrabi, K., Yamani, Z.H., Al-Sulaiman, F.A., 2018b. Performance enhancement of dye-sensitized solar cells via cosensitization of ruthenizer Z907 and organic sensitizer SQ2. *Int. J. Energy Res.* 42, 3957–3965. <https://doi.org/10.1002/er.4154>.
- Yum, J.-H., Jang, S.-R., Walter, P., Geiger, T., Nüesch, F., Kim, S., Ko, J., Grätzel, M., Nazeeruddin, M.K., 2007. Efficient co-sensitization of nanocrystalline TiO₂ films by organic sensitizers. *Chem. Commun. (Camb)* 4680–4682. <https://doi.org/10.1039/b710759e>.